Int. J. High Technology Ceramics **4** (1988) 51–71

The Milling and Densification Behaviour of β′-Sialon Powders Prepared from Alumino-Silicate Minerals

H. Mostaghaci, F. L. Riley*

Department of Ceramics, University of Leeds, Leeds LS2 9JT, UK

&

J.-P. Torre

Céramiques Techniques Desmarquest, 2 Rue Albert Einstein, Trappes 78190, France

(Received 25 October 1987; revised version received 6 February 1988; accepted 18 April 1988)

ABSTRACT

Alumino-silicate minerals are potentially a convenient and low-cost source of β′-sialon powders, gained through high temperature carbothermal reduction under nitrogen. Four β′-sialon powders prepared by this method have been examined for milling behaviour and sinterability. An assessment is made of the effects of trace impurities in the alumino-silicate starting materials, and of the oxygen–nitrogen balance, on the characteristics of the β′-sialon powders.

INTRODUCTION

The controlled high temperature carbon (carbothermal) reduction under nitrogen of readily available naturally occurring alumino-silicate minerals or cheap raw materials such as waste product silica offers the possibility of an economically attractive production route to silicon nitride and related materials of the sialon type. Because these nitride powders are formed from sub-micrometer dimension starting powders by reactions involving vapour phase species, it was expected that they would also conveniently be in a finely divided form and therefore readily sinterable.

Numerous studies of the carbothermal reduction process have been

* To whom all correspondence should be addressed.

Int. J. High Technology Ceramics 0267-3762/88/$03·50

published. Lee & Cutler[1] were the first to describe the reaction of clay–carbon mixtures under nitrogen to form the β'-sialon, $Si_3Al_3O_3N_5$. This reaction can be expressed:

$$3(Al_2O_3 . 2SiO_2 . 2H_2O) + 15C + 5N_2 \rightarrow 2Si_3Al_3O_3N_5 + 15CO + 6H_2O \quad (1)$$

Other reaction equations using oxide materials of different Al_2O_3/SiO_2 ratios and giving sialons of different z-value may similarly be written. The extent of conversion to the nitride is controlled by the proportion of carbon used, and by the reaction conditions. Later studies have described sialons similarly prepared from illite and kaolinite minerals.[2,3]

Factors affecting reaction rates, and possible reaction mechanisms, have been explored in some detail.[4–12] There is convincing evidence that the gas phase species SiO and CO are important, and that the production of nitrides by this type of process involves heterogeneous and gas phase reactions.[9] Metals such as iron, which may be expected to form liquid silicides under reaction conditions, appear to favour the production of silicon carbide.[10] This is particularly the case at temperatures above $\sim$1400°C where the silicon nitride is susceptible to loss of nitrogen:

$$Si_3N_4 + 3C \rightarrow 3SiC + 2N_2 \quad (2)$$

This study has been concerned with the characterisation of an extended range of sialon powders, with the overall objective of testing the quality and behaviour of materials obtained from naturally occurring minerals of different types and Al/Si ratios. Powders of β'-sialon with z-values of 0·8, 2·1 and 2·7 were used. Two types of material with z-values of 0·8 were examined, one obtained from a mixture of kaolinite and silica, the other from a mixture of gibbsite and silica. Relationships between starting oxide composition and sialon composition, as calculated on the basis of analysed Al/Si ratios and measured nitrogen content, are shown in Fig. 1. Hot pressing (pressure sintering) was used as a convenient and rapid means of obtaining a comparative measure of the likely sintering behaviour of a series of related materials. These general findings were substantiated in a selected number of cases by pressureless sintering studies.

Because of the nature of the preparative conditions required for the β'-sialon materials, involving reactions at temperatures of the order of 1500°C, the raw β'-sialon is obtained in the form of lightly sintered blocks of low bulk density. In order to obtain fine powders suitable for conventional powder forming processes the blocks have first to be broken down. The milling treatment required to give adequately fine, sinterable powders formed the basis for the first stage of this study, and yielded information about the structure of the as-received semiparticulate materials. The second stage of the programme concerned the densification behaviour of the milled

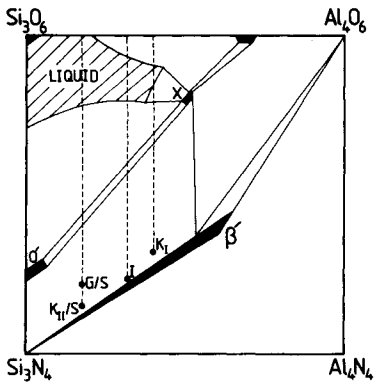

Fig. 1. Abridged schematic diagram of the sialon behaviour diagram for 1700°C showing the relationships between alumino silicate mineral composition and β′-sialon. Key: K_{II}/S = kaolinite (II)-silica, z = 0·8; G/S = gibbsite–silica, z = 0·8; I = illite, z = 2·1; K_I = kaolinite (I), z = 2·7. (See also Tables 1 and 2.)

powders. From both stages of the programme it became clear that the phase and chemical purity of the β′-sialon powders was of considerable importance both for their milling characteristics and for their sinterability.

EXPERIMENTAL

β′-sialon powders were prepared and supplied by Céramiques Techniques Desmarquest, France. The chemical compositions of the starting minerals used are shown in Table 1; sialon materials were received in the as-prepared form of briquettes or small cylinders ~75 mm × 30 mm diameter, and were roughly crushed (<10 mm) prior to further treatment. Carbothermal reduction had been carried out in each case using an approximately 150 ks heating programme in which the temperature of appropriate mineral-carbon mixtures was raised to 1500°C over ~80 ks, and then maintained until carbon monoxide evolution has ceased. The phase compositions of the materials, as shown by X-ray diffractometry (XRD) (Information provided by H. Le Doussal, la Société Française de Céramique, Paris, France.) are given in Table 2.

Nitrogen analyses of these powders were carried out by two independent methods: (i) hydrolysis in fused sodium hydroxide with titration of released ammonia; (ii) vacuum fusion. The results were in satisfactory agreement, and mean values were used in the materials' assessment.

The milling behaviour of the powders was examined using a tungsten carbide lined mill ('Shatterbox', Glen Creston, Stanmore, UK). Batches of 25 g of powder were milled for times ranging from 20 to 600 s. Particle size

TABLE 1
Chemical Compositions of Raw Materials (mass %)

	SiO_2	Al_2O_3	Fe_2O_3	TiO_2	CaO	MgO	Na_2O	K_2O	P_2O_5	ZrO_2	*Ignition loss*
Kaolinite (I)	46·30	34·90	1·90	1·83	0·64	—	—	0·02	0·08	—	13·80
Illite	66·90	21·45	1·02	1·74	0·19	0·13	0·12	1·49	0·04	—	6·98
Kaolinite (II)	47·20	36·90	0·85	0·18	Trace	0·24	0·02	1·00	—	—	13·30
Gibbsite	0·17	65·3	0·054	0·007	0·048	0·005	0·19	0·019	—	—	34·1
Silica	94·70	3·65	0·15	—	Trace	Trace	0·15	0·05	—	1·30	—

TABLE 2
Phase Compositions of β′-Sialon Powders

Powder source	*Nominal z-value*	*Phases detected*[a]
Kaolinite I	2·7	β′-sialon 15R (tr) Si_2N_2O (tr) Al_2O_3 (tr)
Illite	2·1	β′-sialon Al_2O_3 (tr)
Kaolinite II/silica	0·8	β′-sialon
Gibbsite/silica	0·8	β′-sialon

[a] tr = trace.

data were obtained using a Stokes' sedimentation technique ('Sedigraph 500ET', Micromeritics, Norcross, Georgia), and by nitrogen adsorption using a three-point BET method ('Quantasorb', Quantachrome Corporation, Syosset, New York). The compaction behaviour of the powders was evaluated from the cross-head movement in an Instron Universal testing machine (Model 1185, Instron Corporation, High Wycombe, UK) using steel dies and punches. Corrections were made to the strain data to take account of compression in the steel punches.

Powders were hot-pressed with and without yttrium oxide densification aid, under standardised conditions (1700 ± 5°C, $20 \pm 0{\cdot}5$ MPa) in graphite dies coated internally with a thin film of boron nitride powder to reduce any reaction with the graphite. Densification rates were recorded automatically and continuously. The intended pressure was applied to the cold material from a ballast reservoir and then released while the powder was heated. A hot-pressing temperature was reached in ~ 600 s from the cold, the final 200°C being covered in ~ 100 s. Densification shrinkage was automatically recorded ~ 5 s after the reapplication of pressure from the ballast reservoir when the required temperature was reached. Final sialon disc (25 mm diameter, ~ 10 mm thick) densities were determined by a mercury immersion method.

'Pressureless' sintering was carried out in a controlled atmosphere pressure furnace equipped with a dilatometer. A nitrogen pressure of 1·2 MPa was used to suppress dissociation of the sialon, and sintering discs were supported in a hot-pressed boron nitride crucible which also contained loose-packed sialon powder in a 50% mixture with boron nitride powder. A standard temperature of 1700°C was used, which could be attained within 1800 s.

For microstructural examination, polished dense samples were first etched in a 3:1 concentrated phosphoric/sulphuric acid mixture at 200–240°C for 20–120 s. This procedure satisfactorily delineated the main β'-sialon phase by preferentially removing grain-boundary material.

RESULTS

Powder characteristics

Composition

XRD analyses, and measurements of *d*-spacing, showed that the major crystalline phase present in each powder was β'-sialon. Traces of other oxygen and nitrogen containing phases were also detected (Table 2), which indicated that complete high temperature equilibration may not have occurred. Nitrogen analyses are shown in Table 3. All powders contained a small amount of carbon ($1{\cdot}3 \pm 0{\cdot}3\%$), as determined by a vacuum fusion method.

Milling

The effect of milling time on the BET specific surface areas of the four powders is shown in Fig. 2a. These data are also expressed as relative apparent particle dimension as a function of milling time in Fig. 2b. Similar data for particle dimensions of three powders determined by the sedimentation method are shown in Figs 3a and 3b. Particle size distributions determined by the sedimentation method are shown in Figs 4a and 4b for powders milled for 300 s. Figure 5 shows the relationships between Stokes diameter and apparent primary (BET) particle size

TABLE 3
Nitrogen Content (% theoretical) of β'-Sialon Powders

Sialon powder source	*z-value*	*Nitrogen content (% theoretical[a])*		
		Chemical analysis	*Vacuum fusion*	*Mean*
Kaolinite (I)	2·7	77	84	81
Illite	2·1	96	99	98
Kaolinite (II)/silica	0·8	85	92	89
Gibbsite/silica	0·8	73	74	74

[a] For single phase β'-sialon of specified *z*-value.

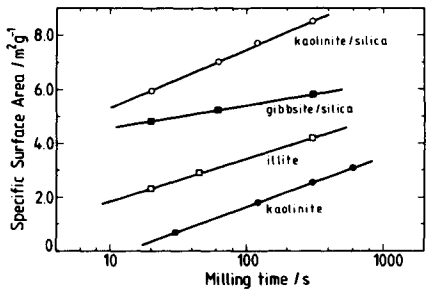

Fig. 2a. BET specific surface area as a function of milling time in a tungsten carbide mill.

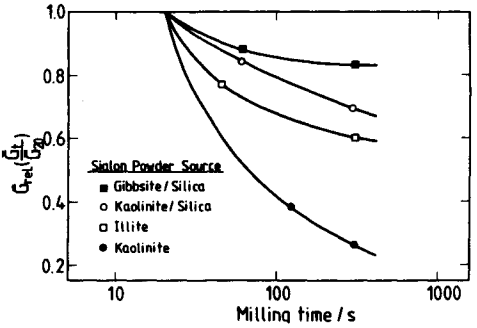

Fig. 2b. Relative apparent particle dimension as a function of milling time; reference point $\bar{G}_{20}$ refers to 20 s milling.

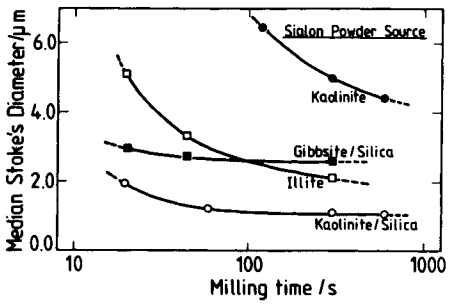

Fig. 3a. Median Stokes' diameter as a function of milling time.

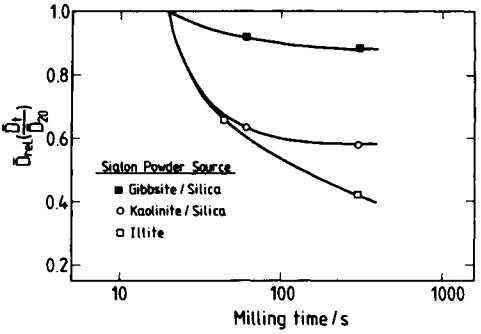

Fig. 3b. Relative Stokes' diameter as a function of milling time; reference point D_{20} refers to 20 s milling.

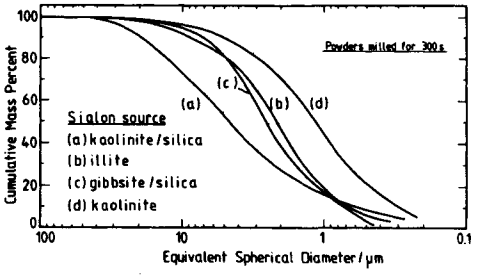

Fig. 4a. Sedimentation particle distribution curves, from water at 25°C.

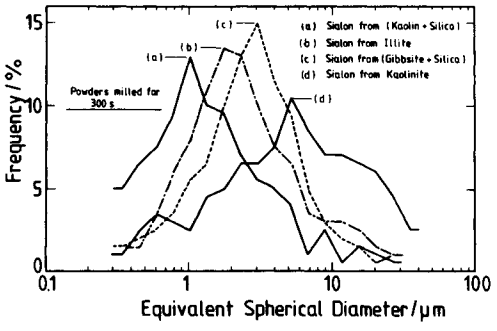

Fig. 4b. Corresponding particle size distribution frequencies.

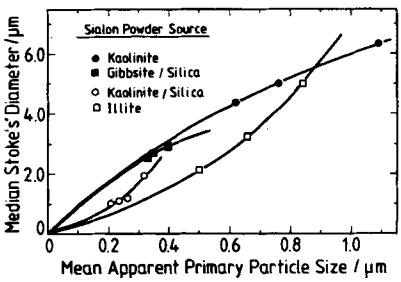

Fig. 5. Median Stokes' diameter expressed as a function of mean apparent (BET) primary particle size.

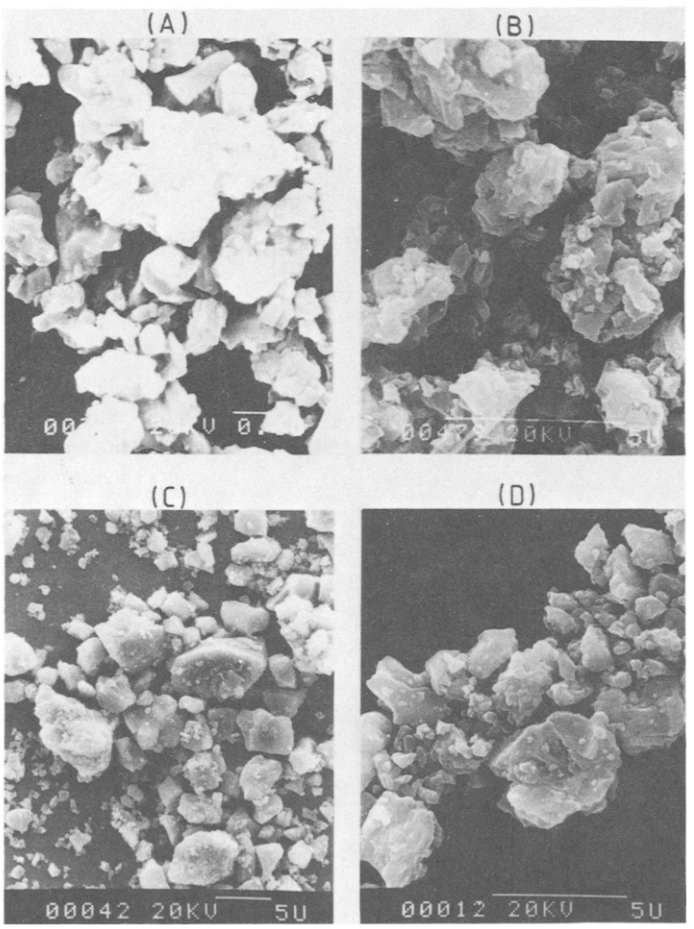

Fig. 6. Scanning Electron Micrographs of β'-sialon powders milled for 300 s; (A) gibbsite–silica; (B) kaolinite (II)-silica; (C) illite; (D) kaolinite (I)

dimensions with increased milling time for each sialon powder. Scanning electron micrographs of powders milled for 300 s are shown in Fig. 6.

Compaction

Data for powder density as a function of compaction pressure are shown in Fig. 7. Green density values calculated from the cross-head movement and final green density (mercury densitometry) were corrected to take into account the slight distortion under load of the punches and die.

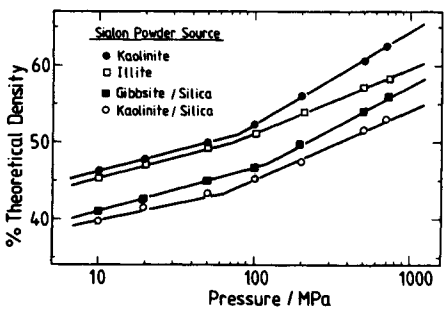

Fig. 7. Powder compaction behaviour under continuous loading; density as a function of log (applied pressure).

Densification

Typical smoothed curves for the hot-pressing densification behaviour of a set of sialon powders of approximately the same particle size, without sintering additives, are shown in Fig. 8, expressed as density as a function of time. The final density values (mercury immersion) were assumed to correspond to theoretical density. These powders had been milled to give similar BET surface areas, in the range 3–6 $m^2 g^{-1}$ (0·6–0·3 μm apparent mean particle size). The higher z-value sialons proved to be difficult to mill to the specific surface areas obtained for the $z = 0{\cdot}8$ sialons (Fig. 2), and slightly coarser, 3 $m^2 g^{-1}$, powders were used for densification studies of the $z = 2{\cdot}1$

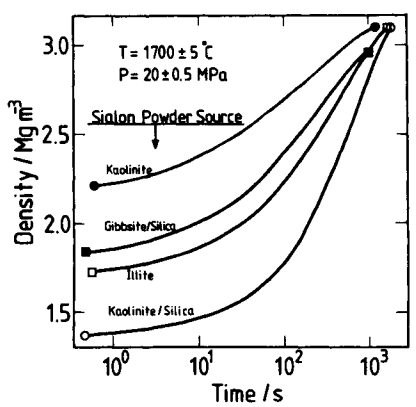

Fig. 8. Hot-pressing densification behaviour at 1700°C of four β′-sialon powders; density as a function of log (time).

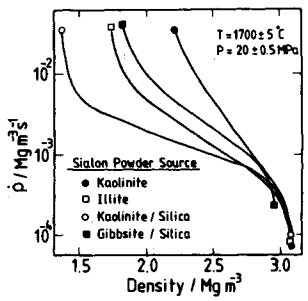

Fig. 9. Hot-pressing densification behaviour at 1700°C; derived densification rate values as a function of density.

and 2·7 sialons. Corresponding plots giving densification rate ($\dot{\rho}$) as a function of density are shown in Fig. 9, where

$$\dot{\rho} = \frac{d\rho}{dt}$$

The influence of yttrium oxide (BDH AR grade) on densification behaviour was examined using 2, 5 and 9 mass percentage additions. The additive was wet-milled (propan-2-ol) into prepared β'-sialon powders and the liquid evaporated with constant agitation. Typical representative data for the gibbsite–silica sialons are given in Figs 10 and 11, showing density as

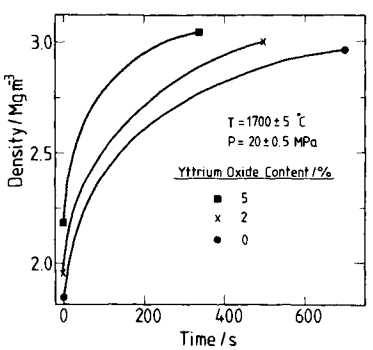

Fig. 10. Hot-pressing densification behaviour of gibbsite–silica, $z = 0{\cdot}8$ β'-sialon powder at 1700°C in the presence of 0, 2 and 5 mass % Y_2O_3.

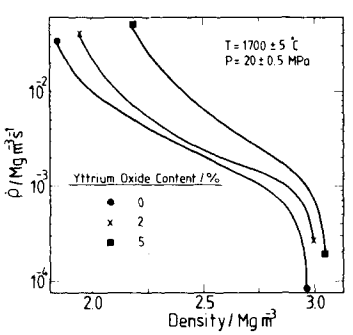

Fig. 11. Hot-pressing densification of gibbsite–silica powder (BET mean particle dimension 0·33 μm) at 1700°C; instantaneous densification rates at 2·5 Mg m^{-3} density as a function of yttrium oxide addition.

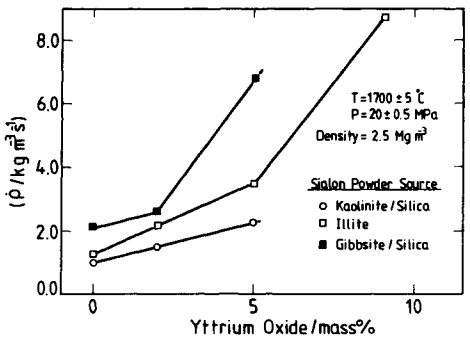

Fig. 12. The effect of yttrium oxide addition on densification behaviour; instantaneous densification rates at 2·5 Mg m^{-3} density as a function of yttrium oxide addition.

a function of time, and densification rate as a function of density. The overall effect of yttrium oxide addition on densification rate at a density of 2·5 Mg m^{-3} is shown in Fig. 12.

Figure 13 shows the pressureless sintering densification behaviour of the $z = 0{\cdot}8$ gibbsite–silica material (initial mean particle size 0·35 μm) sintered at 1700°C with varying additions of yttrium oxide. Figure 14 shows densification curves for the four powders sintered at 1700°C without additive. The mean particle dimensions ($\bar{G}$) of these powders after various milling times are shown in Table 4.

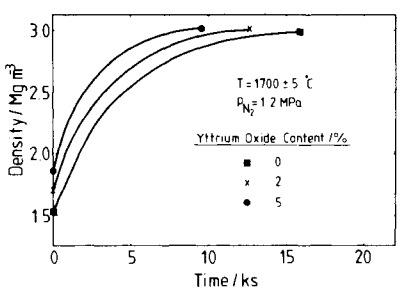

Fig. 13. Pressureless sintering densification of gibbsite–silica powder (BET mean particle dimension 0·3 μm) at 1700°C with Y_2O_3 additions.

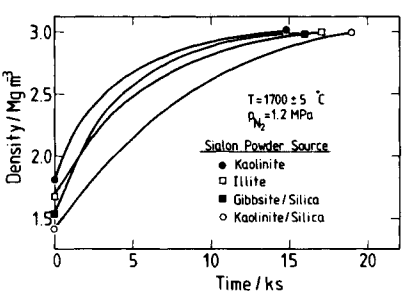

Fig. 14. Pressureless sintering densification of sialon powders without additive, at 1700°C.

TABLE 4
Powders Used for Pressureless Sintering and Hot-pressing

	Milling time (s)	$\bar{G}(\mu m)$	
		Stokes	*BET*
Kaolinite I	600	4·4	0·62
Illite	45	3·3	0·65
Gibbsite-silica	60	2·7	0·35
Kaolinite II-silica	20	1·9	0·32

DISCUSSION

A number of important features has emerged from this study, some expected, some unexpected. In general terms it has been possible to characterise satisfactorily each of the four β'-sialon powders. Each powder has been shown to behave quite differently in certain respects, while retaining broad similarities with the other members of the group. The reasons for these differences have been sought in the nature, and the chemical purity, of the starting oxide materials, and possibly in slight differences of treatment during carbothermal reduction.

It has become quite clear that although the starting materials were of a high specific surface area a considerable reduction in area took place during the conversion to β'-sialon powder. This is believed to be due in part to the nature of the chemical reactions occurring, with consequential partial or complete loss of identity, and hence morphology, of the oxide particles,[6,7] and in part to a liquid phase assisted sintering process involving liquids generated from trace impurity oxides during the reduction stage. The sialon powders obtained were thus initially considerably coarser than the starting materials. This was due in large measure to the formation of hard agglomerates by the primary particles. The agglomerated powders were quite difficult to mill to a higher specific surface area. All powders could, however, be both hot-pressed and sintered to high density, processes which the yttrium oxide additions assisted, but which were also seen to a marked extent in the absence of additional liquid-forming oxides. This indicated that the sialon powders already contained potential liquid-forming materials, the result of the presence of metal oxide impurities, and, in three of the sialon powders, a significant excess of oxygen over the theoretical (for β'-sialon) O/N value. Such oxygen-rich materials are known to sinter in the absence of other sintering aids,[13] more readily than those of theoretical stoichiometry.

The four sialon powders showed markedly differing milling characteristics, and hard agglomerates constructed from 0·2–5 μm primary particles appeared to be an important feature. Initially the largest agglomerates, following light crushing of the briquettes, were found in the kaolinite and illite-derived high z-value materials. This was shown in the Stokes' data. BET surface area data provided a similar picture, though the primary particle dimensions indicated were some 10 × smaller than the agglomerate sedimentation dimensions. Figure 5 summarises this information, and also indicates the pattern of milling behaviour. A more detailed analysis of milling behaviour is provided by the semi-logarithmic graphs in Figs 2(a) and 3(a). However, in view of the range of initial particle dimensions, the response of each powder to the milling is better shown in terms of the relative change in primary and agglomerate particle dimension, shown in Figs 2(b) and 3(b). It can be seen that the kaolinite and illite high z-value, and large initial dimension, agglomerates are the more readily broken down. Both $z = 0{\cdot}8$ powders resist milling, the gibbsite–silica powder being the most difficult. The finest powder, in absolute terms, was the kaolinite–silica, which was initially the finest powder and also susceptible to some further milling breakdown.

This milling information suggests that the least extent of large scale presintering and agglomeration occurs with the two low z-value sialons. The gibbsite–silica material on the other hand appears to contain extremely hard smaller agglomerates, which are difficult to break down further. Those of the kaolinite–silica material are much weaker. Thus, overall, two levels of agglomeration are indicated; one based on 'long-range' weaker bridges forming crushable clusters of particles, the other, based on 'short-range' but much stronger bridges. A schematic diagram illustrating the pattern of agglomeration suggested by this evidence is shown in Fig. 15. This

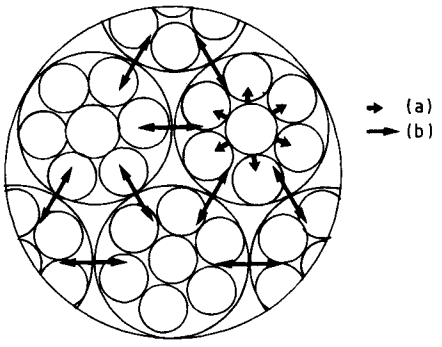

Fig. 15. Schematic of pattern of agglomerate structure within an agglomerate particle as suggested by milling and compaction behaviour: (a) short range strong bridges; (b) longer range weaker bridges. Primary particle dimension ~0·2–0·8 μm. Overall agglomerate dimension ~6 μm, inner hard agglomerate dimension ~2 μm.

TABLE 5
Sialon Agglomerate Apparent Strengths

Material	*z-value*	*Approximate critical pressure (MPa)*
Kaolinite I	2·7	80
Illite	2·1	70
Kaolinite II/silica	0·8	60
Gibbsite/silica	0·8	100

impression is reinforced by the powder compaction data, which also suggest stronger agglomerate units in the gibbsite–silica material, and weak agglomerite units in the kaolinite-silica.[14] The approximate values for the compaction pressure at the points of shape-change obtained from Fig. 7 are shown in Table 5, and in conforming to the pattern of the milling behaviour suggest that the smaller agglomerates are significant for the pressing behaviour.

A further indication of the type of agglomerate feature which may be occurring is given by Fig. 5. The different curvatures of the four lines suggest that the illite and kaolinite–silica particles fracture more evenly to provide two relatively large particles (a relatively small increase in specific surface area for a given decrease in Stokes' dimension). The kaolinite and gibbsite/silica agglomerates on the other hand appear to fracture more unevenly, and provide smaller 'splinter' fragments (a relatively large increase in specific surface area for a given decrease in Stokes' dimension), and to which the BET method would be expected to be sensitive.

All powders densified rapidly under hot-pressing conditions at 1700°C, with full density being reached in ~ 1 ks (Fig. 8). Because of the differences in initial particle size (Table 4) it is possible to make immediate direct comparisons only with the kaolinite–illite and gibbsite/silica–kaolinite/silica pairs. Instantaneous densification rate data obtained from Fig. 9 for a density of 2·50 Mg m^{-3} are shown in Table 6, indicating that the relatively coarse kaolinite ($z = 2{\cdot}7$ sialon) powder densified quickest, and that the fine kaolinite/silica ($z = 0{\cdot}8$) powder has the slowest kinetics. Densification data can, however, be adjusted for particle size differences on the basis of earlier observations on the influence of particle size on densification rate for the kaolinite and illite powders, for which the densification rate–particle size dependence was:

$$\dot{\rho} = K\bar{G}^{n} \tag{3}$$

(where K is a grain dimension independent term and n is an integer), with $n = -1$ for illite and -3 for kaolinite.[15] These exponent values were

TABLE 6
Hot-pressing Instantaneous Densification Rates

β′-sialon source	*z value*	*n*	*Densification rate at density = 2·5 Mg m⁻³; $\dot{\rho}$/Mg m⁻³ s⁻¹*	
			$\dot{\rho}$ observed	*$\dot{\rho}$ adjusted to $\bar{G} = 0{\cdot}3\ \mu m$*
Gibbsite-silica	0·8	−1	0·002 07	0·002 3
Kaolinite II + silica	0·8	−1	0·001 00	0·001 0
Illite	2·1	−1	0·001 21	0·002 5
Kaolinite I	2·7	−3	0·004 81	0·035 0

believed to reflect grain-boundary sliding (low volume of liquid) and solution-recrystallisation (high volume of liquid) control of densification rate, respectively,[16,17,18] and would be consistent with the nature of the two β′-sialon powders, of differing purity levels. The *n* value for the two $z = 0{\cdot}8$ sialons was not determined experimentally but was arbitrarily put at −1. This was initially justifiable in view of the known high purity of these materials, and the expected low liquid phase content. Densification rate data, adjusted on this basis to a 'standard' particle dimension of 0·3 μm, are given in the last column in Table 6. Significant differences exist between the pairs of identical, or similar, *z*-value. Thus the gibbsite–silica $z = 0{\cdot}8$ powder is seen to be densifying at over twice the rate of that derived from the kaolinite–silica mixture; the kaolinite $z = 2{\cdot}7$ sialon is densifying at more than 10 times the rate of the illite $z = 2{\cdot}1$ sialon. The differences in the case of the $z = 0{\cdot}8$ materials would be larger still if an exponent of $n = -3$ for the particle size dependence for densification had been used for the gibbsite–silica material.

A possible explanation for these differences in densification behaviour lies in the purity of the starting materials. Figure 16 shows schematically a

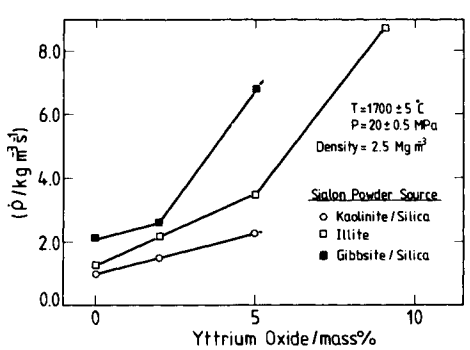

Fig. 16. Instantaneous densification rates at density of 2·5 Mg m⁻³ of sialon powder, corrected for initial particle dimension, in relation to mineral impurity level.

comparison between corrected instantaneous densification rates (at density = 2·5 Mg m^{-3}) and starting mineral purity (mass %). For the low z-value materials based on silica-rich mixtures, values for impurity levels are calculated from those for silica adjusted appropriately for impurities introduced with the small amount of kaolinite required to give the 0·8 z-value (Table 1). The correlations between densification rate and oxide content both for CaO and Fe_2O_3 is strong in the cases of the kaolinite and illite-derived materials. The high purity gibbsite–silica derived material, however, shows fast densification compared with the kaolinite–silica material of the same z-value. In Fig. 16 only the point corresponding to the Fe_2O_3 content is shown (the CaO and TiO_2 contents are close to zero and the corresponding points are omitted). The apparent correlations shown in Fig. 16 may be associated with the formation of calcium aluminosilicate, and ferrosilicon liquids respectively. It would be expected that Fe_2O_3 would be reduced to metallic iron during the carbothermal treatment, subsequently to form $FeSi_x$ (silicon rich eutectic at 1209°C) by reaction with silicon nitride. The apparent lack of correlation with the TiO_2 content can be attributed to the reduction of TiO_2 to inert, and refractory, TiN or TiC. Both the silicate and the ferro-silicon liquids would be expected to assist the sintering process. The reason why the gibbsite–silica powder does not fit the pattern shown by the other three powders may lie in its relatively high oxygen content, and the likely presence therefore of a significantly larger quantity of X-phase liquid under hot-pressing conditions. Thus it would appear that powder purity and the O/N balance are both potentially of importance in determining sinterability; this is not a surprising conclusion.

It is of interest that these observations on the apparent effects of powder purity and O/N balance may also be used to explain the milling behaviour of the sialon powders. In this respect the presence of calcium aluminosilicate, or ferrosilicon liquids during the carbothermal reduction stage of sialon powder preparation would be expected to assist primary particle pre-sintering and agglomeration. There is a clear correlation, shown schematically in Fig. 17, between powder purity and agglomerate hardness expressed as median agglomerate size after a standard (300 s) milling treatment, which links the kaolinite, illite and kaolinite/silica powders. Again the gibbsite–silica powder does not fit well into this pattern (only the Fe_2O_3 point is shown) in providing harder and less easily broken down agglomerates compared with those from the kaolinite–silica derived sialon. A closely similar pattern is shown by comparison of the sialon powder critical crushing loads (Table 5) and mineral oxide impurity levels.

The generally high densification rates shown by the four powders must thus be assumed to be the result of the combination of liquid-forming impurity materials in the powders, together with a tendency for the powders

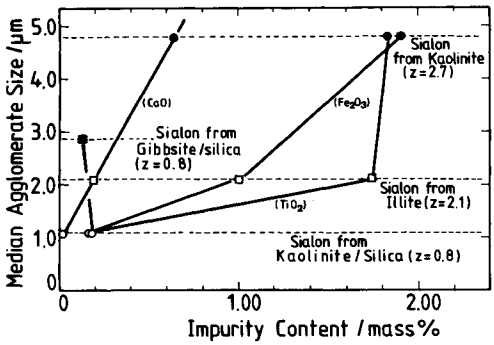

Fig. 17. Median agglomerate size after 300 s milling, shown in relation to mineral impurity level.

to be slightly oxygen rich with respect to the appropriate O/N balance for each z-value. This tendency is marked with the gibbsite–silica powder and appears to more than compensate for the high purity of this material. The reason for this high oxygen level is likely to be the imperfect control of the carbothermal reduction conditions in this particular instance.

The addition of yttrium oxide, at the 2, 5 and 9 mass % level, provides the expected acceleration in densification rate due to the generation of yttrium aluminosilicate liquid to aid liquid phase sintering. This is illustrated in Fig. 11 for the gibbsite–silica material, which can now be densified under standard conditions in $\sim 0{\cdot}5$ ks or less. The overall pattern is illustrated in Fig. 12 for the three most pure sialon powders with densification rates at a density of $2{\cdot}5\ \mathrm{Mg\,m^{-3}}$ plotted against yttrium oxide addition. The effect is most marked in the gibbsite–silica and illite powders, possibly again reflecting the absence of species (SiO_2 for example) able to assist in forming liquids with Y_2O_3 at 1700°C.

Pressureless sintering of the four powders yields maximum density materials after extended sintering times. The kaolinite–silica material is slowest at 1700°C, requiring ~ 20 ks. In the presence of yttrium oxide some acceleration is obtained, illustrated by the curves for the silica powder, Fig. 13. The pattern of behaviour seen with pressureless sintering thus matches precisely that found for hot-pressing. The only slightly surprising feature is the marked sinterability of these powders without additions of sintering aid, indicating the presence of inbuilt and effective liquid-forming phases.

In all materials obtained by hot-pressing and by sintering, memory of the agglomerated nature of the starting powder was retained in the dense microstructure. Etched, previously polished surfaces of typical materials are shown in Fig. 18. These are typical of all sialon materials examined and show evidence for clusters of sialon grains surrounded by regions richer in a second phase material more readily attacked by the etchant. Individual

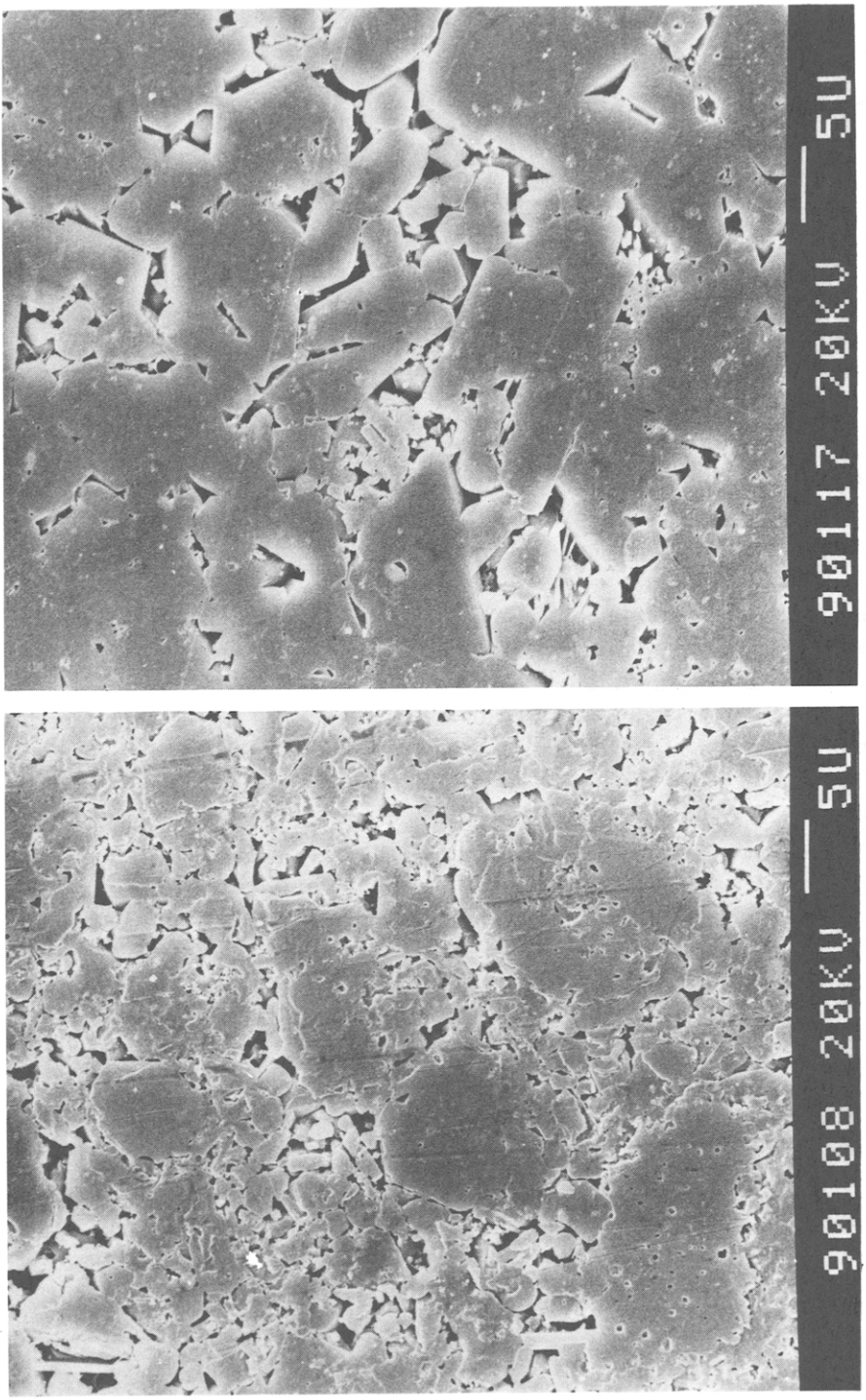

Fig. 18. Chemically etched polished sections of kaolinite (a) and illite (b) sialon materials, after hot-pressing to full density without sintering additive, showing retention of powder agglomerate structure. The location of silicate grain boundary and secondary phase material is indicated by the more deeply etched regions.

grains are small (~0·5–1 μm), but the clusters have a dimension of ~5–10 μm, matching the form of the starting milled sialon powders. This indicates that the small agglomerate particles remain relatively unaffected internally by the liquid phase, which resides for the most part at the larger aggregate boundaries. These features would be expected to have a strong influence on the mechanical properties of these materials, particularly at high temperature.

The mechanical properties of materials prepared by sintering were not determined in this stage of the programme. Preliminary results (Torre, J.-P. & LeDoussal, H., unpublished) with materials of this type suggest that bond strengths at ~25°C well in excess of 300 MPa can readily be obtained. These values, obtained with an essentially prototype and unrefined material, are thus encouraging. Refinement of sintered grain-sizes, and in particular the elimination of the larger agglomerates, are thus primary objectives in the development of higher strength materials.

CONCLUSIONS

β-sialon powders may readily be prepared with a range of z-values from appropriate mixtures of aluminosilicate and silica raw materials. The sialon powders so obtained consist of agglomerates of varying degrees of hardness. The strength of the agglomerate appears to be associated with two factors:

(i) raw material purity, particularly with respect to species able to form liquids during the carbothermal reduction treatment;
(ii) the extent of replacement of O by N during reduction.

The agglomerate sizes are considerably larger than the starting mineral particle sizes, and difficulty may be experienced in milling the powders to an adequate level of fineness. Of the powders examined here the $z = 0{\cdot}8$ powder obtained from the high purity kaolinite–silica mixture was most satisfactory in these respects, in being fine, and yet still fairly readily milled. The small agglomerates obtained from the gibbsite–silica mixtures were exceptionally hard. Because the silica used was the same in these two materials, this difference is attributed to the carbothermal reduction process and slight variations in reducing conditions, possibly temperature and gas flow rate. Accurate temperature control at this stage is in any case important, because of the conflicting needs of containing an adequate degree of reduction in a short time and of avoiding excessive pre-sintering of the developing sialon powders.

All four powders could be pressureless sintered to full density in times of the order of 20 ks at 1700°C without using additional sintering aids, although 5 mass % of yttrium oxide reduced the time required to attain full density by a factor of two. The agglomerate structure of the starting powder tended to be carried through to the final dense microstructure, indicating the importance of avoiding the development of hard agglomerates in the sialon powder by, for example, careful attention to the carbothermal reduction conditions and oxide purity. With one exception (the illite-derived powder) the O/N balances were slightly high, suggesting that control over the reduction stage had been inadequate. It is thus clear that of optimum powder quality is to be obtained, further detailed studies of the carbothermal reduction stage of the process are needed, to enable the process to be refined through improved understanding of the controlling parameters.

The possibility of preparing sinterable, high purity β'-sialon powders from naturally occurring or readily available low-cost raw materials has been demonstrated. Although these materials have not yet been fully developed, reasonable quality fine-grain microstructure can be obtained. This suggests that commercial low-cost sialon materials of a quality matching or significantly better than presently available conventional oxide and nitride materials should soon be within reach.

ACKNOWLEDGEMENTS

Dr E. Gilbart and Mr Q. Fan provided advice and invaluable experimental assistance. The collaboration of H. LeDoussal of the Société Française de Céramique in this programme is gratefully acknowledged. This work was part-funded by DG XII of the Commission of the European Communities.

REFERENCES

1. Lee, J. G. & Cutler, I. B., Sinterable sialon powder by reaction of clay with carbon and nitrogen. *Am. Ceram. Soc. Bull.*, **58** (1979) 869–71.
2. Mostaghaci, H., Fan, Q., Riley, F. L., Bigay, Y. & Torre, J. P., The development of microstructure in sialons prepared from aluminosilicate minerals. *Br. Ceram. Trans. J.*, **85** (1986) 12–16.
3. Van Dijn, F. K., Betselaar, R. & Siskens, C. A. M., Reaction-rate limiting steps in carbothermal reaction processes. *J. Am. Ceram. Soc.*, **68** (1985) 16–19.
4. Paris, R. A. & Grollier-Baron, T., Procédé de préparation de sialons, produits obtenus et articles fabriques de ces produits. European Patent 23869, 2 Nov. 1981.

5. Van Dijn, F. K., Siskens, C. A. M. & Metselaar, R., Carbothermal production of β′-sialon. In *Science of Ceramics Vol. 12*, ed. P. Vincenzini. Ceramurgica s.r.l., Faenza, Italy, 1984, pp. 427–33.
6. Siddiqi, S. A., Higgins, I. & Hendry, A., Production of β′-sialon by carbothermal reaction of clay. In *Proceedings of the International Conference Non-oxide technical and engineering ceramics*, ed. S. Hampshire. Elsevier, London, 1986, p. 119.
7. Zhang, S-C. & Cannon, W. R., Production of silicon nitride from silica. *J. Am. Ceram. Soc.*, **67** (1984) 691–5.
8. Szweda, A., Hendry, A. & Jack, K. H., The preparation of silicon nitride from silica by sol-gel processing. In *Proceedings of the British Ceramic Society, Vol. 31*, eds D. Taylor & P. Popper. British Ceramic Society, Stoke-on-Trent, 1981, pp. 107–18.
9. Lee, J. G. & Cutler, I. B., Formation of silicon carbide from rice hulls. *Am. Ceram. Soc. Bull.*, **54** (1975) 195–8.
10. Siddiqi, S. A. & Hendry, A., The influence of iron on the preparation of silicon nitride from silica. *J. Mat. Sci.*, **20** (1985) 3230–8.
11. Higgins, I. & Hendry, A., In Novel Ceramic fabrication processes and applications, ed. R. J. Davidge, Institute of Ceramics, Stoke-on-Trent, 1987, p. 163.
12. Higgins, I. & Hendry, A., Production of β′-sialon by carbothermal reduction of kaolinite. *Trans. J. Brit. Ceram. Soc.*, **85** (1986) 161.
13. Benn, M. & Riley, F. L., Observations on the reaction sintering of compositions in the system Al–Si–N–O. *J. Mat. Sci.*, **15** (1980) 529.
14. Niesz, D. E., Bennett, R. B. & Snyder, M. J., Strength characterization of powder aggregates. *Bull. Amer. Ceram. Soc.*, **51**(9) (1972) 677–80.
15. Mostaghaci, H., Fan, Q., Riley, F. L., Bigay, Y. & Torre, J. P., The development of microstructure in sialons prepared from alumino silicate minerals. *Rev. Int. Hautes Temps. Refract. Fr.*, **22** (1985) 208.
16. Langdon, T. G., In *Deformation of Ceramic Materials*, ed. R. C. Bradt & R. E. Tressler. Plenum Press, New York, 1975, p. 101.
17. Bowen, L. J., Weston, R. J., Carruthers, T. G. & Brook, R. J., Mechanisms of densification during the pressure sintering of alpha-silicon nitride. *Ceramurgia Int.*, **2**(4) (1976) 173–6.
18. Rahman, M. N. A., Riley, F. L. & Brook, R. J., Mechanisms of hot-pressing in the system Si–Al–O–N. *J. Amer. Ceram. Soc.*, **63** (1980) 648.